

Frustrated matryovska-doll synchronization and emergent complexity on the human connectome network.

Pablo Villegas,¹ Paolo Moretti,¹ and Miguel A. Muñoz¹

¹*Departamento de Electromagnetismo y Física de la Materia e Instituto Carlos I de Física Teórica y Computacional. Universidad de Granada, E-18071 Granada, Spain*

The spontaneous emergence of coherent behavior through synchronization plays a key role in neural function and performance, and its anomalies often lie at the basis of pathologies. Here we study analytically and computationally the synchronization (Kuramoto) dynamics on the actual human-brain connectome network. Between the synchronous and asynchronous regimes that can be achieved by tuning details in any generic network, here we elucidate the existence of a novel, broad intermediate state, stemming from the hierarchical modular organization of the connectome. Where one would expect a hierarchical matryovska-doll synchronization process, we show that the interplay between network structure and quenched node frequency heterogeneity gives rise to frustrated synchronization, metastability, and chimera states. We uncover the spectral origin of the dynamic freezing behind such phenomenology, and discuss how such complex synchronization patterns relate to the need for the brain to access large dynamical repertoires without *ad hoc* fine-tuning to a critical point.

Neuro-imaging techniques have recently allowed the reconstruction of structural human brain networks, composed of hundreds of neural regions and thousands of interconnections consisting of white matter fibres. The resulting “human connectome” (HC) [1, 2] is structured in moduli—with a much larger intra than inter connectivity—organized in a hierarchical fractal-like fashion across many scales [3–8]. On the other hand, “functional” connections between nodes in these networks have been inferred from correlations in neural activity as detected in EEG or fMRI time series. Unveiling how structural and functional networks influence each other is a task of outmost importance. In this context, a few pioneering works found that the hierarchical-modular organization of structural brain networks has profound implications for neural dynamics [7, 9–12]. For example, neural activity propagates in hierarchical networks in a rather distinctive way, not observed on simpler network architectures [13]; beside the usual two phases—percolating and non-percolating—commonly exhibited by models of activity propagation, an intermediate “Griffiths phase” [14] emerges on the HC network [13, 15]. This novel phase stems from the existence of highly-diverse relatively-isolated moduli or “rare regions”, where dynamical activity remains mostly localized giving rise to anomalously slow dynamics and critical-like response [13, 15].

As brain function requires coordinated or coherent neural activity at a wide range of scales, synchronization is one of the major themes in neuroscience [16, 17]. Neuronal synchronization plays a key role in vision, memory and other cognitive functions [18], as well as in pathologies such as epilepsy [19]. Our goal here is to scrutinize the special features of synchronization dynamics [20]—as exemplified by the canonical Kuramoto model [21–23]—running on top of the actual HC network [1, 2, 24]. This consists of a set of 998 nodes, each of them representing a population of neurons producing self-sustained oscillations

[25], whose mutual connections are encoded by a symmetric weighted connectivity matrix \mathbf{W} [1, 2]. Here, we shall uncover the existence of a novel intermediate phase for synchronization dynamics—stemming from the hierarchical modular organization of the HC— and identify it as the optimal regime for the brain to harbor complex behavior, large dynamical repertoires, and optimal trade-offs between local segregation and global integration.

The Kuramoto dynamics on a generic network (see [24] for a nice review) is defined by

$$\dot{\theta}_i(t) = \omega_i + \frac{k}{N} \sum_{j=1}^N W_{ij} \sin [\theta_j(t) - \theta_i(t)], \quad (1)$$

where $\theta_i(t)$ is the phase at node i at time t . The intrinsic frequencies ω_i —accounting for heterogeneity—are extracted from some arbitrary distribution function $g(w)$, W_{ij} are the elements of the $N \times N$ connectivity matrix \mathbf{W} , and k is an overall coupling parameter. Time delays, noise, and phase frustration could also be simply implemented. The Kuramoto order parameter is defined by $Z(t) = R(t)e^{i\psi(t)} = \langle e^{i\theta_i(t)} \rangle$ where $0 \leq R \leq 1$ gauges the overall coherence and $\psi(t)$ is the average phase. In the absence of frequency dispersion coherence always emerges ($R > 0$) while, with frequency heterogeneity, and for large populations of well-connected oscillators, the model exhibits a phase transition at some critical value of k , separating a coherent steady state from an incoherent one ($R = 0$, plus $N^{-1/2}$ corrections) [21–24]. The time-dependence can also be tackled analytically by using the celebrated Ott-Antonsen (OA) ansatz, allowing for a projection of the high-dimensional dynamics onto an evolution equation for $Z(t)$, with remarkable accuracy in the large- N limit [26, 27]. We have conducted a computational analysis of the Kuramoto model on top of the HC network. As illustrated in Fig.1, between the coherent

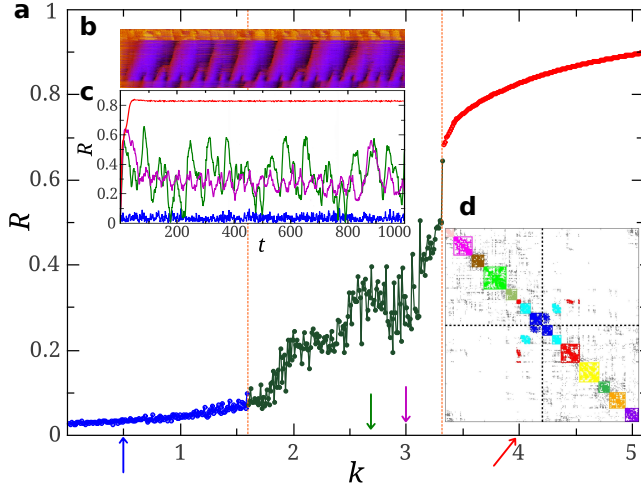


FIG. 1: (Color online) a) Time average of the order parameter $R(t)$, for Kuramoto dynamics on the HC network for a specific and fixed set of frequencies extracted from a $N(0, 1)$ Gaussian distribution. A broad intermediate regime separates the incoherent phase (low k) from the synchronous one (high k). In this, coherence increases with k in an intermittent fashion, and with strong dependence on the frequency realization. b) Raster plot of individual phases showing local rather than global synchrony and the coexistence of coherent and incoherent nodes ($k = 2.7$). c) $R(t)$ for 4 values of k (arrows in the main plot). d) Adjacency matrix of the HC network. Nodes are reordered to emphasize the modular structure highlighted by the community detection algorithm (main text), keeping the partition into the 2 hemispheres (dashed lines). Intra-modular connections (shown in color) are dense while inter-modular ones (grey) are limited to tiny subsets, acting as interfaces between moduli. Integration between moduli is mostly carried out by the 3 central moduli.

and incoherent phase, we find an extended intermediate regime. This is characterized by broad quasi-periodic temporal oscillations of $R(t)$. Anomalously large sampling times would be required to extract good statistics and results depend wildly upon the specific realization of intrinsic frequencies. Collective oscillations of $R(t)$ are a manifestation of partial synchronization and are robust against changes in the frequency distribution (e.g. Lorentz, uniform, etc.) and the normalization convention for the coupling k , whereas the location and width of the intermediate phase depend upon details. As this phenomenology is reminiscent of Griffiths phases –posed in between order and disorder and stemming from rare-region effects [13–15]– it is natural to wonder how the structural network modularity affects synchronization dynamics.

Any network with perfectly isolated moduli, independently synchronized, will exhibit oscillations of $R(t)$, with peaks at times when maximal mutual synchronization is incidentally achieved. Such oscillations can become chaotic if a finite and relatively small number of different coherent moduli are coupled together [28]. Thus, in a connected network without delays or other additional

ingredients, oscillations in the global coherence are the trademark of a strong modular structure, in which moduli are weakly interconnected. This is, indeed, the case of the HC network for which an organization into differentiated hierarchical levels is revealed by standard community detection algorithms [8, 29]. For instance, the optimal partition into communities –i.e. the one maximizing the modularity parameter [30]– corresponds to a division in 12 communities (see Fig.1d). At a higher hierarchical level, a separation into just 2 moduli –corresponding to the 2 cerebral hemispheres– is obtained [2] (Fig.1d). Although more levels of hierarchical partitioning can be inferred (giving rise to a full dendrogram), for the sake of simplicity, we focus in the two levels, $l = 1$ (12 moduli) and $l = 2$ (2 moduli), respectively. To shed

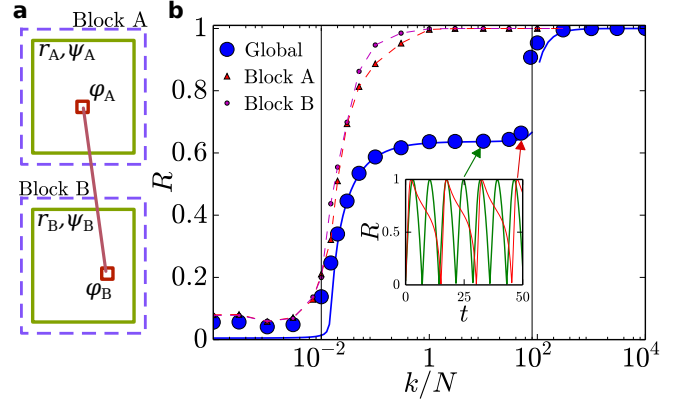


FIG. 2: (Color online) (a) Sketch of the two-block model. (b) Global order parameter for the two-block model with $M = 128$. Results of the numerical integration of the 256 Kuramoto equations (blue points) are in strikingly good agreement with the integration of Eqs.(3) (solid blue line). Local block-wise order parameters are shown for comparison (small symbols; dashed lines are guides to the eye). A first transition, where local order emerges, occurs at $k \approx 2$, while global coherence is reached at a larger value of k . In the intermediate region, the global $R(t)$ oscillates (inset), revealing the lack of global coherence.

light on the properties of synchronization on this peculiar community-structured network, we consider a simple network model consisting of a few blocks with large internal connectivity and very sparse inter-connectivity. Each block is composed by a bulk of $M \gg 1$ nodes that share no connection with the outside and a relatively small “interfacial” set that connects with nodes in other blocks. For instance, in the simplest possible example of just two blocks connected by a single pair of nodes (see Fig.2) each block is endowed with local coherence $r_{A,B}$, average phase $\psi_{A,B}$, and average characteristic frequency $\omega_{A,B}$, while 1-node interfaces have perfect coherence $r = 1$, phase $\varphi_{A,B}$, and characteristic frequency $\nu_{A,B}$. The OA formalism can be safely applied to each single block (large M) but not to interfaces. In the particular case in which

characteristic frequencies are extracted from Lorentz distributions with zero average and spreads $\delta_{A,B}$ (allowing to reach analytical results), the resulting equations are

$$\begin{aligned}\dot{\psi}_A &= \omega_A + \frac{k}{N} \frac{1+r_A^2}{2r_A} \sin(\varphi_A - \psi_A) \\ \dot{r}_A &= -\delta_A r_A + \frac{k}{N} \frac{1-r_A^2}{2} [Mr_A + \cos(\varphi_A - \psi_A)] \\ \dot{\varphi}_A &= \nu_A + \frac{k}{N} [Mr_A \sin(\psi_A - \varphi_A) + \sin(\varphi_B - \varphi_A)]\end{aligned}\quad (2)$$

(coherence $r = 1$ is fixed for each 1-node interface), and a symmetric set of equations ($A \leftrightarrow B$) for block B. The solution of Eq.(2) is displayed in Fig.2; it reveals the existence of a transition to local coherence within each block at a certain threshold value of k . As soon as local order is attained, $r_{A,B} \approx 1$ and $\dot{\psi}_{A,B} \approx 0$, from Eq.(2) the mutual synchronization process obeys $\dot{\varphi}_A \approx (\nu_A + M\omega_A) + \frac{k}{N} \sin(\varphi_B - \varphi_A)$ and a symmetrical equation for $\dot{\varphi}_B$. The right-hand side is dominated by $\nu_A + M\omega_A$: whereas the average value ω_A becomes arbitrarily small within blocks (with large M), the frequency ν_A does not. Consequently, synchronization between the two blocks through the interfacial link is frustrated by these non-vanishing interfacial frequencies: each block remains internally synchronized but it is unable to achieve coherence with the other over a broad interval of coupling strengths. This interval is delimited above by a second transition at $k/N \sim \max\{M|\omega_{A,B}|, \nu_{A,B}\}$, whereas k is large enough as to overcome frustration and global coherence emerges. This picture is confirmed by numerical integration of the full system of N coupled Kuramoto equations as well as by its OA approximation (Eq.(2)), both leading to remarkably similar results. Thus, local and global coherences emerge at two well-separated transition points. In the intermediate range, R oscillates (Fig.2), as occurs for the HC network. An analysis similar to ours, but considering many blocks and much stronger inter-connections, revealed two separate transitions as well, but with no sign of an oscillatory phase in between [27]: the existence of “structural bottlenecks” between moduli and its interplay with heterogeneously distributed frequencies is essential for overall oscillations to emerge. Summing up, the two-block model exemplifies the concept of structural frustration—which is key to the rest of the paper—as the basic mechanism responsible for the emergence of oscillations in the global coherence. Still, this two-block model—with only one hierarchical level—is far too simple to account for all the rich phenomenology emerging on the HC, as illustrated in what follows. **Local-coherence oscillations in the HC**—Fig.3 shows numerical results for the local order parameter $r^{(l)}$ for either the coarser partition in 2 moduli ($l = 2$) or the finer one into 12 of them ($l = 1$). It reveals that (Fig.3a) local coherences exhibit oscillatory patterns in time (with characteristic frequencies typically between

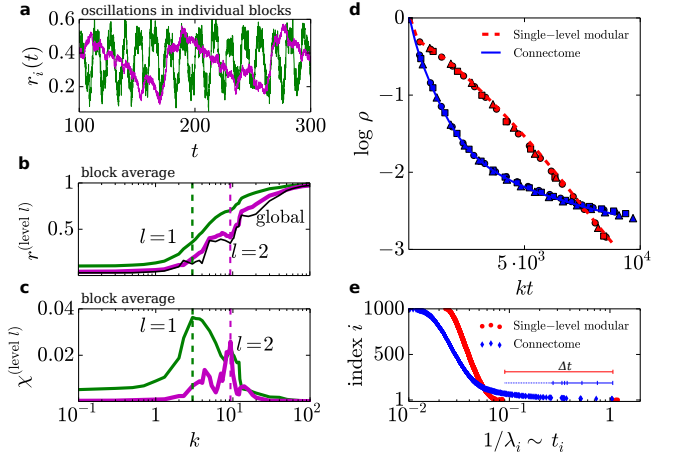


FIG. 3: (Color online) a) Oscillations of the local order parameters (“chimera states”) in one particular modulus in the partitions of the HC into 12 (green; $k = 3$) and 2 (magenta; $k = 10$) moduli, respectively. b) Average local order parameter and c) chimera index for blocks at levels as in a), as a function of k . Global order (thin black line in b)) emerges only after local order is attained at lower levels. d) Average decay of activity ρ for identical frequencies $\omega = 0$ and comparison with a single-level modular network (made up of 4 similar random moduli at a single hierarchical level) of the same size and average connectivity as the HC network. Symbols stand for different values of k . e) Characteristic times corresponding to the inverse of the first 1000 non-trivial eigenvalues of the Laplacian matrix (x axis) as a function of their respective ordered indices (y axis), for networks as in d). The stretched exponential behavior in d) is the result of the convolution of slow time scales associated with small eigenvalues in e).

0.01 and 0.1 Hz) and that (Fig.3b) the transition to local coherence at progressively higher hierarchical level occurs at progressively larger values of k ; i.e. coherence emerges out of a hierarchical bottom-up process as in a nested sequence of two-block models (see [31]). Indeed, structural frustration, as introduced above, affects all hierarchical levels; as every modulus encloses sub-moduli and a finer-grain structure at a lower scale, local coherences are expected to exhibit oscillations at all hierarchical levels (as shown in Fig. 3a). The average variance of r (called chimera index, χ) [32] exhibits a marked peak at each hierarchical level—reflecting maximal configurational variability—at its corresponding synchronization transition (Fig.3b-c). Similar intra-modulus oscillatory patterns—dubbed *chimera states*—have been recently found [25, 32, 33] in Kuramoto models in which the presence of delays or explicit phase lags induces a different kind of explicit frustration, hindering global synchronization. Remarkably, the chimera states put forward here have a purely structural origin. Fig.3b also reveals that the ordering process may be non-monotonous: coherence does not systematically grow with k . The emergence of local order in some community may hinder or reduce coherence at others, inducing a local “desynchronization”,

reflecting the metastable nature of the explored states.

Slow dynamics and spectral properties on the HC network— We have shown that heterogeneous frequencies frustrate the synchronization process at structural bottlenecks. The situation in which frequencies are assumed to be identical, instead, allows us to focus on structural effects alone. Let us consider, without loss of generality, the simplest case $\omega_i = 0$, and define the activity $\rho = 1 - \langle R \rangle$. Perfect asymptotic coherence, $\rho = 0$, is expected to emerge regardless of k . However, as illustrated in Fig.3d, the convergence towards $\rho = 0$ is very slow (slower than exponential and much slower than for a single-level modular network). This can be analytically investigated assuming that, for large enough times, all phase differences are relatively small. Then, up to first order, $\dot{\theta}_i = -\kappa \sum_j L_{ij} \theta_j$, where $\kappa = k/N$ and $L_{ij} = \delta_{ij} \sum_l W_{jl} - W_{ij}$ are the elements of the Laplacian matrix ([34] and refs. therein), whose spectrum controls the asymptotic dynamics. Indeed, $\theta_i(t) = \sum_{l,j} e^{-\kappa \lambda_l t} v_i^l v_j^l \theta_j(0)$, where λ_l denotes the l -th Laplacian eigenvalue ($0 = \lambda_1 < \lambda_2 < \dots < \lambda_N$) and v_i^l the i -th component of the corresponding eigenvector. Given that $Z(t) \approx \sum_j (1 + i\theta_j - \frac{1}{2}\theta_j^2)/N$, averaging over initial conditions, and considering that—as the Laplacian has zero row-sums [34]— $\lambda_1 = 0$, we obtain that $\rho(t) = \frac{\sigma^2}{2} \sum_{l=2}^N e^{-2\kappa \lambda_l t}$, where σ is the standard deviation of the initial phases, and which holds for any generic network. As usual, the larger the “spectral gap”, λ_2 , the more “entangled” the network and thus the more difficult to divide it into well separated moduli (indeed, $\lambda_2 = 0$ only for disconnected networks) [34]. For large spectral gaps all timescales are fast, and the last expression can be approximated by its leading contribution, ensuing exponential relaxation to $\rho = 0$, as in fact observed in well-connected network architectures (Erdős-Rényi, scale free, etc. [30]). This is not the case for the HC matrix, for which λ_2 is much smaller than, e.g. in the simple modular networks studied above (see Fig.3e) and a tail of small non-degenerate eigenvalues is encountered (see Fig.3d and [13]). Each eigenvalue, λ_i in this tail corresponds to a division of moduli into sub-moduli [34], and the broad tail reflects the existence of a rich hierarchical modular structure. Each of these eigenvalues—with its associated large timescale, $t_i = 1/\lambda_i$ —contributes to the sum above, giving rise to a convolution of relaxation processes entailing anomalously-slow dynamics. A simple single-level modular network made up of a few similar moduli does not account for slow relaxation (see Fig.3d-e): slow dynamics stems from the existence of a hierarchy of moduli and structural bottlenecks.

Hierarchical modular synthetic networks — To shed light on these findings for the HC—frustration, chimera states, and slow dynamics—we study more complex and realistic underlying network architectures: hierarchical modular networks (HMN) in which moduli exists within moduli in a nested way [3–8]. This is a sort of two-

block model in which each of the two blocks is on its turn composed of a smaller two-block subsystem. HMN are assembled in a “bottom-up” fashion: local fully-connected moduli (with e.g. of 16 nodes) are used as building blocks. They are recursively grouped by establishing additional inter-moduli links in a level-dependent way as sketched in Fig.4(top) [13, 35]. Computer simulations of

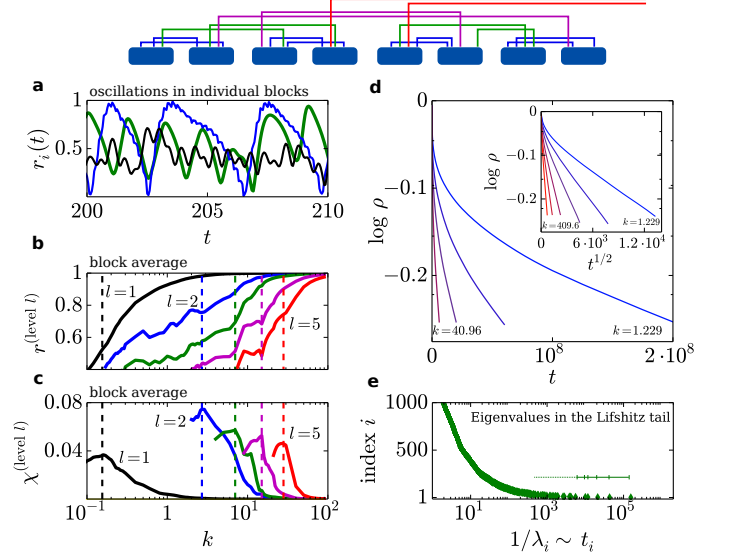


FIG. 4: (Color online) HMN networks. Top panel: sketch of the HMN model. At hierarchical level 1, 2^s basal fully connected blocks of size M are linked pairwise into super-blocks by establishing a fixed number α of random links between the elements of each ($\alpha = 2$ in the Fig.). Newly formed blocks are then linked iteratively with the same α up to level s , until the network becomes connected. a), b), c) as in Fig.3, but for a HMN with $N = 512$, $s = 5$, and $\alpha = 4$. Hierarchical levels are $i = 1 \rightarrow 5$ in black, blue, green, magenta and red respectively (not all shown in a) for clarity). d) Time relaxation of activity ρ for homogeneous characteristic frequencies $\omega = 0$, for logarithmically equispaced values of k . Averages over $> 10^6$ network realizations of HMNs with $N = 4096$ and $s = 11$. Inset: as in the main plot d), but representing as a function of $t^{1/2}$, confirming the predicted stretched exponential behavior. e) Inverse tail-eigenvalues (as in Fig.3) for a HMN as in e).

the Kuramoto dynamics on HMN substrates (see Fig.4) reveal: (i) the existence of a sequence of synchronization transitions for progressively higher hierarchical levels at increasing values of k , (ii) chimera states at every hierarchical level, resulting in a hierarchy of metastable states with maximal variability at the corresponding transition points, (iii) slow relaxation to the coherent state when all internal frequencies are identical, and (iv) anomalies in the Laplacian spectrum analogous to those of the HC network. Indeed, for these HMNs, the lower edge of the Laplacian spectrum has been shown [13] to be characterized by a continuous exponential Lifshitz tail $p(\lambda) \sim e^{-1/\lambda^a}$, with $a \approx 1$ for $N \rightarrow \infty$. This implies

that $\rho(t) = \frac{\sigma^2}{2} \int d\lambda p(\lambda) e^{-2\kappa\lambda t}$, yielding $\rho(t) \sim e^{-\sqrt{8\kappa}t}$, i.e. anomalous stretched-exponential behavior, in excellent agreement with computational results (see Fig.4d).

Summing up, in the absence of frequency dispersion, perfect coherence is achieved by following a bottom-up ordering dynamics in which progressively larger communities –with inherently different timescales– become coherent (see [31]). This matryovska-doll synchronization process is constrained structural bottlenecks, bringing about anomalously-slow dynamics at very large timescales. The HC, in spite of being a coarse-grained mapping of a brain network, already shows strong signals of this ideal hierarchical architecture. On the other hand, in the presence of intrinsic frequency dispersion the slow ordering process is further frustrated: inter-moduli frequency barriers need to be overcome before moduli achieve mutual coherence and the system becomes trapped into metastable states with traits of local coherence at different hierarchical levels. The result is a complex synchronization landscape, which is especially rich and diverse in the intermediate regime put forward here. Including ingredients –such as explicit phase frustration [32] or time delays [25, 33]– should only add complexity to the structural frustration effect reported here.

Addition of noise to the Kuramoto dynamics would allow the system to escape from metastable states, making it able to explore the nested hierarchy of attractors, and allowing to rationalize the complex synchronization patterns in real brain networks. Spontaneous dynamical fluctuations have indeed been observed in human brains during quiet rest, defining a “resting state” baseline as evidenced by a wide range of neuro-imaging techniques [36]. This spontaneous activity is characterized by very slow fluctuations, $< 0.1Hz$ (in agreement with our results) and is correlated across different segregated structures. During rest, the brain is routinely exploring different states or attractors. This spontaneous switching could be due to stochastic transitions from one attractor to another, thereby configuring a dynamical state with a large dynamical repertoire [37]. To enhance the possibility of excursions into these attractors it has been suggested that brain networks should operate close to a critical point, to allow for intrinsic large fluctuations entailing attractor “surfing”, and giving access to varied functional configurations [37, 38]. The existence of multiple attractors and noise-induced surfing is largely facilitated in the broad intermediate regime elucidated here, implying that a precise fine tuning to criticality is not strictly required for complex dynamics to emerge: the role usually played by a critical point is largely assumed by a broad intermediate region in hierarchically architected complex systems. Finally, our results might be of relevance for other hierarchically organized systems such as gene regulatory networks for which coherent activations are believed to play a pivotal role.

We acknowledge financial support from J. de An-

dalucía, grant P09-FQM-4682 and we thank O. Sporns for providing us access to the human connectome data.

- [1] P. Hagmann *et al.*, PLoS Biol **6**, e159+ (2008).
- [2] C. J. Honey *et al.*, Proc Natl Acad Sci **106**, 2035 (2009).
- [3] E. Bullmore and O. Sporns, Nat. Rev. Neurosci. **10**, 186 (2009).
- [4] O. Sporns, *Networks of the Brain* (MIT Press, Cambridge, 2010).
- [5] M. Kaiser, NeuroImage **57**, 892 (2011).
- [6] D. Meunier, R. Lambiotte, and E. Bullmore, Front Neurosci **4**, 200 (2010).
- [7] C. Zhou *et al.*, Phys Rev Lett **97**, (2006).
- [8] M. Ivković, K. Amy, and R. Ashish, PLoS ONE **7**, e35029 (2012).
- [9] C. Zhou *et al.*, New J Phys **9**, 178 (2007).
- [10] M. Kaiser, M. Goerner, and C. Hilgetag, New J Phys **9**, 110 (2007).
- [11] C. H. M. Kaiser, Frontiers in Neuroinform. **4**, 14 (2010).
- [12] M. Rubinov, O. Sporns, J.-P. Thivierge, and M. Breakspear, PLoS Comput Biol **7**, e1002038 (2011).
- [13] P. Moretti and M. A. Muñoz, Nat. Commun. **4**, (2013).
- [14] T. Vojta, J Phys A **39**, R143 (2006).
- [15] M. A. Muñoz, R. Juhász, C. Castellano, and G. Ódor, Phys Rev Lett **105**, 128701 (2010).
- [16] G. Buzsáki, *Rhythms of the Brain* (Oxford University Press, NY, 2006).
- [17] M. Breakspear and C. J. Stam, Phil. Trans. R. Soc. Lond. B **360**, 1051 (2005).
- [18] P. N. Steinmetz *et al.*, Nature **404**, 187 (2000).
- [19] E. R. Kandel, J. H. Schwartz, and T. M. Jessell, *Principles of Neural Science* (McGraw-Hill, New York, 2000).
- [20] M. G. Rosenblum, A. Pikovsky, and J. Kurths, *Synchronization – A universal concept in nonlinear sciences* (Cambridge University Press, Cambridge, 2001).
- [21] Y. Kuramoto, Lecture Notes in Physics **39**, 420 (1975).
- [22] S. H. Strogatz, Physica D: **143**, 1 (2000).
- [23] J. A. Acebrón *et al.*, Rev. Mod. Phys. **77**, 137 (2005).
- [24] A. Arenas *et al.*, Physics Reports **469**, 93 (2008).
- [25] J. Cabral, E. Hugues, O. Sporns, and G. Deco, NeuroImage **57**, 130 (2011).
- [26] E. Ott and T. M. Antonsen, Chaos **18**, 037113 (2008).
- [27] P. S. Skardal and J. G. Restrepo, Phys.Rev.E **85**, 016208 (2012).
- [28] O. V. Popovych, Y. L. Maistrenko, and P. A. Tass, Phys. Rev. E **71**, 065201 (2005).
- [29] J. Duch and A. Arenas, Phys. Rev. E **72**, 027104 (2005).
- [30] M. Newman, SIAM Review **45**, 167 (2003).
- [31] A. Arenas, A. Díaz-Guilera, and C. Pérez-Vicente, Phys Rev Lett **96**, 114102 (2006).
- [32] M. Shanahan, Chaos **20**, 013108 (2010).
- [33] M. Wildie and M. Shanahan, Chaos **22**, 043131+ (2012).
- [34] L. Donetti, F. Neri, and M. A. Muñoz, JStat **2006**, P08007 (2006).
- [35] S.-J. Wang, C. C. Hilgetag, and C. Zhou, Front Comput Neurosci **5**, 30 (2011).
- [36] B. Biswal, F. Zerrin Yetkin, V. Haughton, and J. Hyde, Magnetic resonance in medicine **34**, 537 (1995).
- [37] G. Deco and V. K. Jirsa, The Journal of Neuroscience **32**, 3366 (2012).
- [38] D. R. Chialvo, Nature Phys **6**, 744 (2010).